The Kuramoto-Sivashinsky equation: A bridge between PDE'S and dynamical systems

Article *in* Physica D Nonlinear Phenomena · January 1986

DOI: 10.1016/0167-2789(86)90166-1

2 authors, including:

James Mac Hyman
Tulane University
306 PUBLICATIONS **14,493** CITATIONS

SEE PROFILE

Physica 18D (1986) 113–126
North-Holland, Amsterdam

THE KURAMOTO–SIVASHINSKY EQUATION: A BRIDGE BETWEEN PDE'S AND DYNAMICAL SYSTEMS

James M. HYMAN and Basil NICOLAENKO
Center for Nonlinear Studies, Theoretical Division, MS B284, Los Alamos National Laboratory, Los Alamos, NM 87545, USA

Dedicated to Martin Kruskal whose pioneering work combining analytic and computational analysis to unravel the soliton structure in the KdV equation inspired our exploration into the dynamics of the Kuramoto–Sivashinsky equation.

Through extensive numerical simulation, we have characterized the transition to chaos of the solutions to the Kuramoto–Sivashinsky equation. The attracting solution manifolds undergo a complex bifurcation sequence including multimodal fixed points, invariant tori, traveling wave trains, and homoclinic orbits. We relate this behavior to earlier work where the Kuramoto–Sivashinsky equation was shown to behave as a finite dimensional dynamical system of ordinary differential equations.

1. Introduction

We present some preliminary results from a systematic numerical investigation of the transition to chaos of the Kuramoto–Sivashinsky (K–S) equation in one space dimension:

$$u_t + \nu u_{xxxx} + u_{xx} + \tfrac{1}{2}(u_x)^2 = 0,$$
$$(x,t) \in \mathrm{R}^1 \times \mathrm{R}_+, \tag{1.1}$$
$$u(x,0) = u_0(x), \quad u(x+L,t) = u(x,t),$$

where the subscripts indicate partial differentiation, ν is positive, and u_0 is L-periodic, L being the size of a typical pattern cell. The natural bifurcation parameter is the renormalized dimensionless parameter $\tilde{L} = L/(2\pi\sqrt{\nu})$.

The K–S equation models pattern formations in different physical contexts and is a paradigm of low-dimensional behavior in solutions to partial differential equations (PDEs). Kuramoto [11–13] derived it in the context of angular-phase turbulence for a system of reaction–diffusion equations modeling the Belouzov–Zabotinskii reaction in three space dimensions. He considered $u(x_1, x_2, x_3, t)$ to be a small perturbation of a global periodic solution, just beyond the parameter domain where the Hopf bifurcation has occurred. Sivashinsky [16, 25, 26] derived it independently to model small thermal diffusive instabilities in laminar flame fronts. In this case, $u(x_1, x_2, t)$ is the perturbation of an unstable planar flame front in the direction of propagation.

The equation also arises in modeling small perturbations from a reference Poiseuille flow of a film layer on an inclined plane (Benney [3], Lin [14], Pumir [21]). In the specific limit of large nondimensional surface tension, Sivashinsky and Michelson [27] proved that this model reduces to the K–S equation for $w(x,t) = \nabla u(x,t)$:

$$w_t + \nu w_{xxxx} + w_{xx} + w w_x = 0, \tag{1.2}$$

for (x,t) in $\mathrm{R}^1 \times \mathrm{R}_+$, with periodic boundary conditions. The interface elevation $w(x,t)$ is assumed to be small in comparison with the film thickness.

Babchin et al. [2] derived eq. (1.2) as a general mechanism modeling the nonlinear saturation of instabilities in flowing films. For example, in a

0167-2789/86/$03.50

Rayleigh–Taylor-type instability, the combined action of flow shear and surface tension is the dominant saturation mechanism.

The solutions to the K–S equation are characterized by the coexistence of coherent spatial structures with temporal chaos. Previous numerical solutions have exhibited periodic cellular patterns. These cells behave in a periodic fashion for small values of $\tilde{L}$; then as the parameter $\tilde{L}$ is increased, they become chaotic. This has been first evidenced in the two-dimensional computations of Michelson and Sivashinsky [16, 27]. Aimar [1], Manneville, Pomeau, Pelce and Pumir [21–23] investigated the behavior of the solution to the one-dimensional case with Neumann boundary conditions as a function of an increasing cell size L. They observed strange attractors (with positive Lyapunov exponents). The authors observed the low modal behavior of the solution; this led Nicolaenko et al. [17–20] to conjecture that the number of determining (Fourier) modes is proportional to the cell size L. Previously, Pomeau et al. [23] also conjectured a similar proportionality for the dimension of the strange attractor. There is strong numerical evidence that the infinite dimensional solution space for the K–S equation is spanned by the solutions to a coupled system of ordinary differential equations (ODEs) with a few degrees of freedom.

In this article we report on a systematic numerical study of the transition to chaos of the K–S equation. High precision was necessary because of the extreme sensitivity of the simulations to numerical accuracy. Nonconverged numerical solutions of eq. (1.1) can occur in regimes we are interested in if the time integration errors are greater than 10^{-6} per unit time-step. In fact, small effects of the order of 10^{-6} in the energy for some sensitive Fourier modes critically impact on the nonlinear dynamics. To alleviate this, we use a high-precision pseudospectral approximation to the spatial derivatives [9, 10] and a variable time-step, variable order integration method in time to keep the solution errors between 10^{-8} and 10^{-10} per unit time.

A typical example of the extreme numerical sensitivity of the numerical solutions to the K–S equation is the disappearance of homoclinic orbits if the precision is too low. The orbital solution dynamics degenerate into fixed point with a numerically artificial basin of attraction. Our numerical results differ from some of the previous published simulations that relied on second-order schemes with only modest control over time integration errors. For example, Manneville's [15] conclusion that the solution to eq. (1.1) with periodic boundary conditions exhibits only metastable chaos followed by trapping into a stable fixed point is at odds with our calculations.

Another motivation for this study is the recent demonstration by Foias, Nicolaenko, Sell, and Temam [5, 6] that the K–S equation is strictly equivalent to a low-dimensional dynamical system. That is, all orbits are attracted exponentially to a finite-dimensional, bounded, compact, smooth manifold, and the interesting dynamics take place on this "inertial" manifold (see section 3). This implies that the transition to chaos of the K–S equation can be analyzed using the tools developed for low-dimensional dynamical systems.

Our numerical results show a wealth of attractors and invariant manifolds, many of them coexisting for the same bifurcation parameter. We also evidence the pervasiveness of homoclinic orbits and their coexisting cohorts, the invariant attracting tori.

2. Overview of theoretical results

The solution to the K–S equations is characterized by a second-order unstable diffusion term, a fourth-order stabilizing viscosity, and a quadratic nonlinear coupling term. This is reflected in the spectrum of eq. (1.1) linearized about $u \equiv 0$. The eigenfunctions are the Fourier modes $\exp(2\pi i/L)k \cdot x (k \in Z)$, and the corresponding eigenvalues are

$$\Lambda_k = \nu(2\pi k/L)^4 - (2\pi k/L)^2 = (k/\tilde{L})^2\left[(k/\tilde{L})^2 - 1\right]/\nu, \tag{2.1}$$

for $k \in \mathrm{N}$. Therefore, the trivial solution $u \equiv 0$ is unstable as soon as L is large enough.

There are $N = [\tilde{L}]$ positive eigenvalues governing the linear instability (here $[x]$ is the integer part of x). A nontrivial steady state exists for $\tilde{L} \geq 1$. Numerical experiments indicate that these steady states coexist with solutions having complicated oscillatory behavior. Windows of intermittencies are also observed. Nevertheless, computations confirm that $\|\nabla u(t)\|^2$ remains bounded in the L^2 norm, albeit highly oscillatory (outside windows). The linearly unstable low modes are stabilized by the strong nonlinear coupling $\frac{1}{2}|\nabla u|^2$ with the extremely stable high modes.

In a series of papers, Nicolaenko, Scheurer and Temam [17–20] analyze the nonlinear stability of the solution by investigating the global dynamical properties of eq. (1.1). Fo even periodic solutions, they prove the uniform boundedness of orbits and the constructive estimate in the L^2 norm:

$$\lim_{t \to \infty} \sup \left\| \frac{\partial u}{\partial x}(t) \right\| \leq \text{Const } \nu^{-1/4} \tilde{L}^{5/2} \tag{2.2}$$

(containing an absolute constant independent of parameters). Following the Yorke–Kaplan-type inequalities developed by Constantin, Foias and Temam [4], they obtain explicit upper bounds for the Hausdorff dimension d_{H} and the fractal dimension d_{F} of all attractors X of the K–S equation:

$$d_{\mathrm{H}}(X) \leq d_{\mathrm{F}}(X) \leq 1 + \text{const } \tilde{L}^{13/8}, \tag{2.3}$$

again with an absolute constant. These bounds are sharpened [20] by extending a remarkable Sobolev-type inequality obtained by Lieb and Thirring (the later was used by Ruelle in the context of Navier–Stokes chaos [24]) to give

$$d_{\mathrm{H}}(X) \leq d_{\mathrm{F}}(X) \leq 1 + \text{const } \nu^{9/40} \tilde{L}^{3/2}. \tag{2.4}$$

This improved estimate contains a dependence upon the viscosity ν.

Results such as eqs. (2.3) and (2.4) are obtained from estimates for the Lyapunov exponents associated with the flow generated by eq. (1.1), via the Yorke–Kaplan inequalities [4]. The Lyapunov exponents characterize the averaged infinitesimal ellipsoidal deformation of an infinitesimal hypersphere originally at $t = 0$ and transported along the flow. The deformation of this hypersphere can be computed using the trace operator formulas for the linearized flow.

Extending concepts and techniques for global inertial manifolds first developed by Foias and Sell, recently Foias, Nicolaenko, Sell and Temam [5, 6] have established the existence of a unique compact inertial manifold for the K–S equations. To understand this concept, let $\mu_k = (2\pi k/L)^4$, $k = 1, 2, \ldots$, the increasing sequence of eigenvalues of the fourth spatial derivative, with the appropriate boundary conditions. Let P_n be the orthogonal projection of $L^2(0, L)$ on the linear subspace generated by the eigenfunctions associated with the eigenvalues μ_k, $1 \leq k \leq N$ (these are, of course, Fourier modes). Let Q_n be the infinite dimensional projection $Q_n = I - P_n$.

Then M is an N-dimensional inertial manifold of eq. (1.1) if

i) it is the graph of a Lipschitz continuous application Φ: $P_n L^2(0, L) \to Q_n H^1(0, L)$;

ii) M has a compact support and is invariant with respect to the flow defined by eq. (1.1);

iii) all orbits of eq. (1.1) in $H^1(0, L)/\mathrm{R}$ are attracted exponentially to M.

In a rough sense, M is a "global center manifold," with $H^1(0, L) - M$ corresponding to a global infinite-dimensional stable manifold. In refs. 3, 6, it is proved that such a manifold M exists for eq. (1.1), with a dimension

$$d_{\mathrm{in}} < \text{const } \tilde{L}^{3.75} + 1. \tag{2.5}$$

Thus, the dynamics of eq. (1.1) are exponentially asymptotically equivalent to those of a finite-dimensional dynamical system on M. The existence of M itself is a corollary of deep geometric "squeezing" properties for the relative distance between any two solution orbits of eq. (1.1).

Table I
The attracting solution manifolds for the solution to eq. (3.1)

$0 \leqq \alpha \leqq 4$ $0 \leqq \tilde{L} \leqq 1$	0 is a global attractor
$4 \leqq \alpha \leqq 17.30$ $1 < \tilde{L} \leqq 2.08$	global attractor, essentially unimodal fixed point: $a_1 \cos x + \varepsilon a_2 \cos 2x + \varepsilon^2 a_3 \cos 3x + \cdots$
$17.30 \leqq \alpha \leqq 22.50$ $2.08 \leqq \tilde{L} \leqq 2.37$	periodic orbit
$22.50 \leqq \alpha \leqq 43$ $2.37 \leqq \tilde{L} \leqq 3.28$	essentially bimodal globally attracting fixed point: $a_2 \cos 2x + \varepsilon a_4 \cos 4x + \varepsilon^2 a_6 \cos 6x + \cdots$
$43 \leqq \alpha \leqq 54$ $3.28 \leqq \tilde{L} \leqq 3.67$	oscillatory and/or chaotic orbits
$54 \leqq \alpha \leqq 68$ $3.67 \leqq \tilde{L} \leqq 4.12$	essentially trimodal globally attracting fixed point: $a_3 \cos 3x + \varepsilon a_6 \cos 6x + \varepsilon^2 a_9 \cos 9x + \cdots$
$68 \leqq \alpha \leqq 94$ $4.12 \leqq \tilde{L} \leqq 4.85$	oscillatory and/or chaotic orbits
$94 \leqq \alpha \leqq 117.3$ $4.85 \leqq \tilde{L} \leqq 5.415$	essentially quadrimodal globally attracting fixed point: $a_4 \cos 4x + \varepsilon a_8 \cos 8x + \varepsilon^2 a_{12} \cos 12x + \cdots$
$117.3 \leqq \alpha \leqq ?$ $5.415 \leqq \tilde{L} \leqq ?$	chaotic orbits

3. Overview of computational simulations

We have normalized the K–S equation to an interval of length 2π; set the damping parameter to the original value derived by Sivashinsky, $\nu = 4$, and introduced the bifurcation parameter $\alpha = 4\tilde{L}^2$. The equation can now be written as

$$u_t + 4u_{xxxx} + \alpha\left[u_{xx} + \tfrac{1}{2}(u_x)^2\right] = 0,$$
$$0 \leq x \leq 2\pi, \tag{3.1}$$
$$u(x + 2\pi, t) = u(x, t), \quad u(x,0) = u_0(x).$$

This equation is equivalent to eq. (1.1) with a different time scaling.

The mean value of the solution to eq. (3.1)

$$m(t) = \frac{1}{2\pi}\int_0^{2\pi} u(x,t)\,\mathrm{d}x \tag{3.2}$$

satisfies the drift equation

$$\dot{m}(t) = \frac{-\alpha}{4\pi}\int_0^{2\pi}(u_x)^2\,\mathrm{d}x. \tag{3.3}$$

To normalize this drift to zero, we numerically solved the equation for

$$v(x,t) = u(x,t) - m(t). \tag{3.4}$$

That is,

$$v_t + 4v_{xxxx} + \alpha\left[v_{xx} + \tfrac{1}{2}(v_x)^2\right] + m(t) = 0. \tag{3.5}$$

Our preliminary bifurcation catalogue of the attractors to eq. (2.5) is shown in table I and fig. 1. This diagram was created by scanning the interval $0 \leq \alpha \leq 120$, i.e., $0 \leq \tilde{L} = 5.48$. For a fixed α, we searched for different attractors by varying the initial conditions. We systematically tracked the

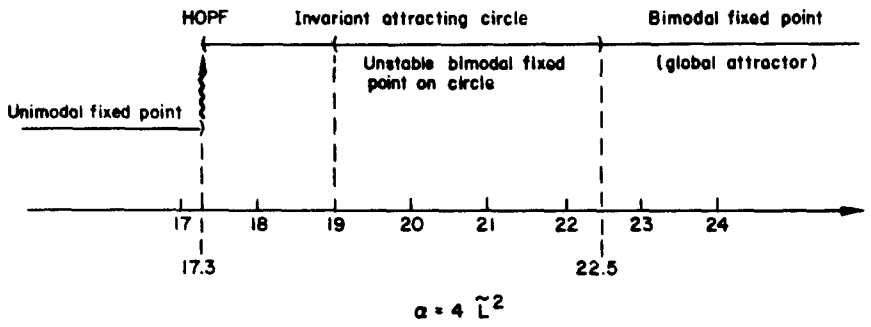

Fig. 1a. The stable solution manifolds have a simple structure when α is small.

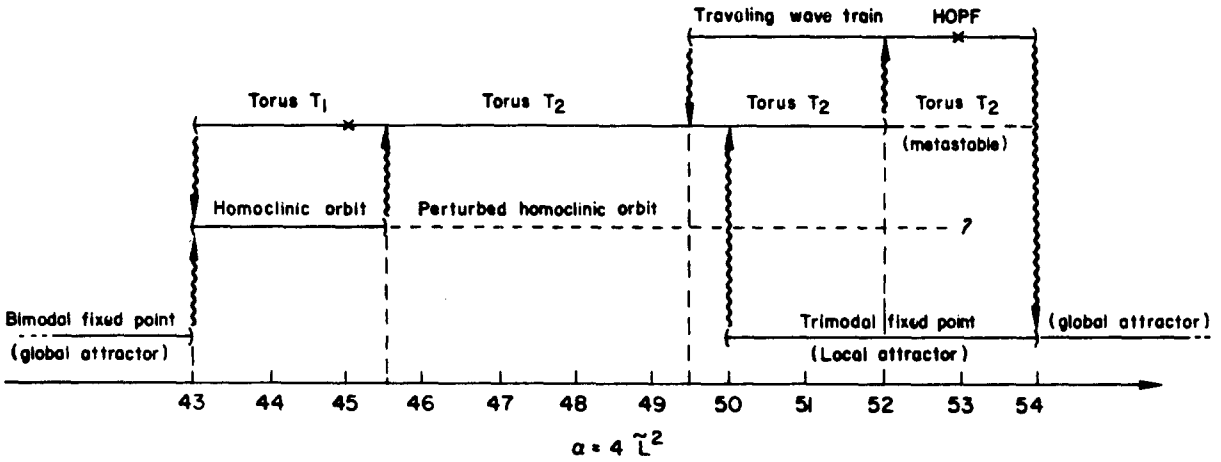

Fig. 1b. As the bifurcation parameter increases, the stable solution manifolds become more complex.

domains of stability of each attractor with respect to the bifurcation parameter by varying α and reinitializing $v(x,0)$ to the final solution from the previous run with a different α.

A remarkable feature of the K–S equation is the alternating windows containing laminar behavior (fixed point, globally attracting) and windows of oscillatory and/or chaotic behavior. The jth laminar window is characterized by a fixed point $\tilde{u}_j(x)$ dominated by $\cos jx$. The higher harmonics of $\cos jx$ have Fourier coefficients decreasing in geometric progression:

$$\tilde{u}_j(x) = a_{1_j}\cos jx + \varepsilon a_{2_j}\cos 2jx + \varepsilon^2 a_{3_j}\cos 3jx + \cdots .$$

Numerically we have found that $a_i = \mathcal{O}(1)$ and $\varepsilon \approx 10^{-1}$. (These are related to the cellular modes discussed by U. Frisch [7].)

Near the boundary of the jth and $(j+1)$st windows of oscillatory and/or chaotic behavior is a competition between a fixed point dominated by $\cos jx$ and the next one dominated by $\cos(j+1)x$. This competition creates a complex interplay between temporal chaos and spatial coherence. In some sense, the (low-dimensional) temporal chaos corresponds to adjustment from one (low-dimensional) space pattern to the next one. We conjecture that as j increases, the bandwidth of the laminar jth window very quickly decreases and one is left with a near continuum of chaos and turbulence.

Starting with $j = 2$, each oscillatory window is dominated by the complex interplay between perturbed homoclinic orbits and invariant tori. We have resolved the second window ($43 \leq \alpha \leq 54$) (cf. fig. 1b) and will give some preliminary results at the onset of the fourth window ($\alpha \geq 117.3$), where positive Lyapunov exponents have been previously computed [23].

The first sequence of bifurcations is a classical (fig. 1a) pitchfork bifurcation at $\tilde{L} = 1$ ($\alpha = 4$) and a Hopf bifurcation at $\tilde{L} = 2.08$ ($\alpha = 17.30$). Nevertheless, the sequence does not lead to further bifurcations and transition to chaos. The invariant circle remains globally attracting, yet a metastable bimodal fixed point (repelling source) appears. At $\alpha = 22.50$ ($\tilde{L} = 2.37$), this fixed point becomes a sink and leads to the second laminar window.

The second oscillatory window (cf. fig. 1b) appears at $\alpha = 43$ ($\tilde{L} = 3.28$) where the bimodal fixed point becomes hyperbolic with a homoclinic loop orbit. A torus T_1 coexists with this homoclinic orbit yet is *not* associated with any Hopf bifurcation. We always observe the transitions: bimodal fixed point $\rightarrow$ homoclinic loop and $T_1 \rightarrow$ homoclinic loop but never bimodal fixed point $\rightarrow T_1$. These transitions are, of course, typical of homoclinic loops [8].

The perturbed homoclinic orbit is observed until $\alpha = 52$; beyond that, complex oscillatory motion takes place, with the accoutrements of chaos. We suspect that the motion is on a perturbed transverse homoclinic orbit.

The torus T_1 bifurcates at $\alpha \approx 45$ into T_2. This T_2 breaks up at $\alpha = 52$. The exact nature of this breakup must still be resolved through Poincaré sections.

To further simplify things, a stable traveling wave train appears at $\alpha = 49.5$ and undergoes its own Hopf bifurcation at $\alpha = 53$. This traveling wave train is correlated to neither the previous bimodal fixed point nor to the new trimodal fixed point. Rather it seems to be a special orbit on the torus T_2.

Last but not least, the trimodal fixed point has a *limited* basin of attraction starting at $\alpha = 50$ and becomes a *global* attractor at $\alpha = 54$ ($\tilde{L} = 4.12$).

Thus, for every α in this window, we have two, if not three, attractors. There is a complex interplay between a perturbed (transversal) homoclinic orbit spurting from the bimodal fixed point and a torus T_2 with its own peculiar dynamics.

We have observed similar mechanisms at the onset of the fourth oscillatory/chaotic window, at $\alpha = 117.5$ ($\tilde{L} = 5.42$), which exhibits a much more definite transverse homoclinic orbit.

4. Selected numerical examples

Several hundred numerical experiments were performed to support the claims made about the dynamics of the asymptotic solutions. In the calculations, we used discrete Fourier transform pseudospectral approximations to the spatial derivatives [9, 10] on grids ranging from 64 to 256 mesh points in single precision (14 digits) on a Cray XMP computer. The solution was integrated in time using a variable order, variable time-step method of lines code, MOLID [10], that retained an absolute error tolerance between 10^{-6} and 10^{-10} per unit time. The runs presented here took between 10^4 and 10^5 time steps. Many problems were recalculated several times with different grid resolutions and time truncation error criteria to ensure that the numerical solutions were converged within an acceptable accuracy.

In the discussion below, the energy is the integral of $(v_x)^2$ and the energy in mode k is the modulus of the kth Fourier coefficient.

The first example (fig. 2) is of an unstable bimodal fixed point imbedded on a globally attracting invariant circle (cf. fig. 1a), which arose from the Hopf bifurcation at $\alpha = 17.30$. The selected case is for $\alpha = 22.3$, $\tilde{L} = 2.36$. In fig. 2a (energy vs. time), we see that the orbit spends a long time in a small neighborhood of the bimodal fixed point solution $\tilde{u}(x) = 2.95 \cos 2x + 0.28 \cos 4x + \cdots$ and then quickly travels around the invariant circle. Fig. 2b (energy in mode 1 vs. time) confirms that the fixed point is bimodal. The energy in mode 1 is small except during bursts when the orbit wraps around the circle. Fig. 2c

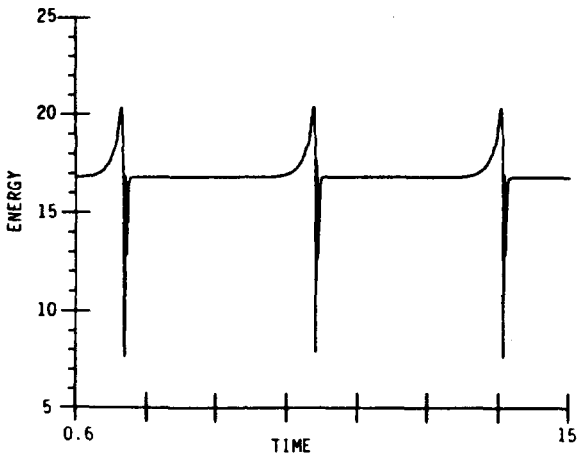

Fig. 2a. The energy of the solution has periodic bursts ($\alpha = 22.3$).

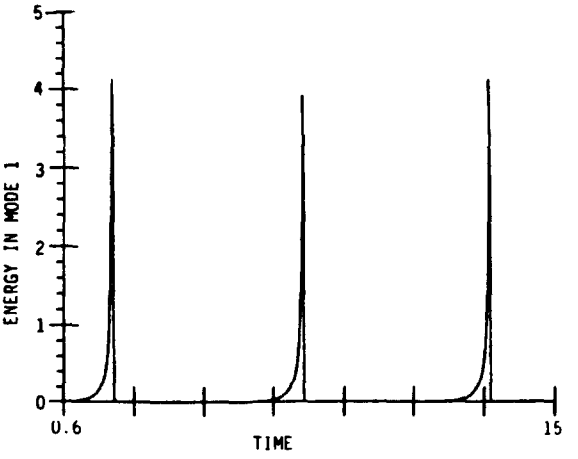

Fig. 2b. The energy in the first mode decays almost to zero during the quiescent bimodal transients.

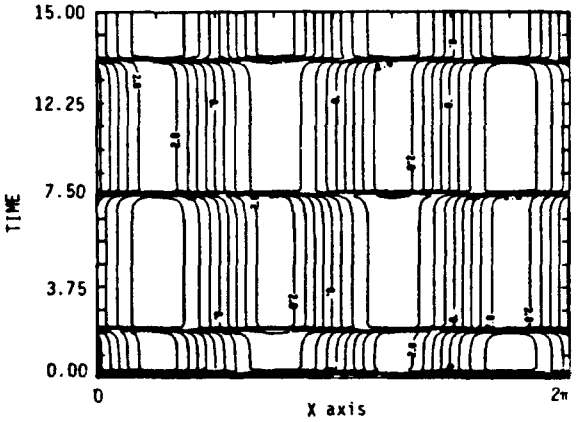

Fig. 2c. The (x, t) contour plots of the solution show a periodic phase shift at the bursts.

[contour levels of $v(x,t)$] indicates that the motion on the circle is periodic with $T \approx 5.6$. As $\alpha \to 22.5$, we observed that the period between bursts monotonically increases to infinity and the fixed point becomes a globally attracting sink.

The next three cases sample the oscillatory window $43 \le \alpha \le 54$. In fig. 3 [$\alpha = 44$, $\tilde{L} = 3.31$, $u_0(x) = 0.1(\cos x + \sin x)$], there is evidence of a suspected homoclinic orbit. In fig. 3a, the orbit spends a substantial time in a neighborhood of the hyperbolic (bimodal) fixed point

$$\tilde{u}(x) = 2.25\cos 2x + 0.59\cos 4x + 0.063\cos 6x + \cdots$$

before bursting around the homoclinic loop. The motion around the loop is triggered by a very sensitive nonlinear exchange of energy between the odd and even modes. In fig. 3b, the energy in mode 1 bursts quickly from 10^{-7} to $\mathcal{O}(1)$. Here an infinitesimal amount of energy (10^{-6}) triggered the burst around the homoclinic loop. A corresponding dip is observed in the energy of mode 2 (fig. 3c). A similar variation for the energy in all the odd modes, $\cos(2j+1)x$, is observed. The contour plot of the solution in fig. 3d indicates that the motion around the homoclinic loop is roughly periodic ($T \approx 0.51$).

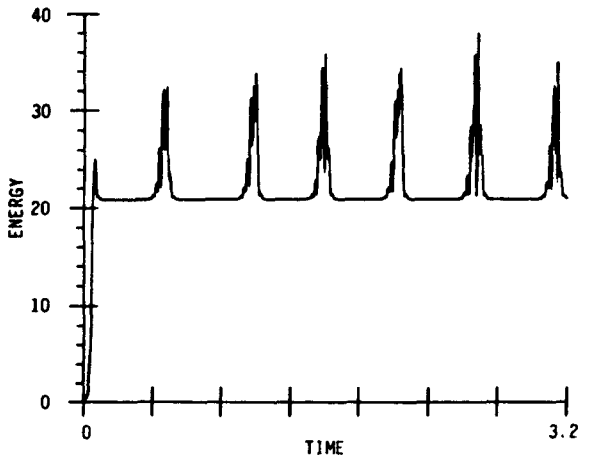

Fig. 3a. The energy in the $\alpha = 44$ solution bursts with a shorter period than in fig. 2, where $\alpha = 22.3$.

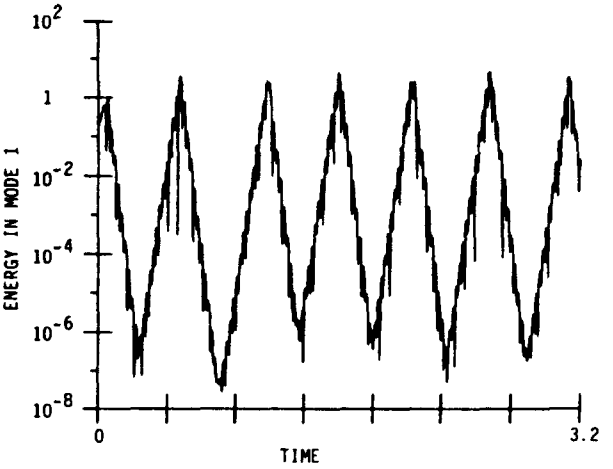

Fig. 3b. The energy in the first mode oscillates over a range of 10^{-6}.

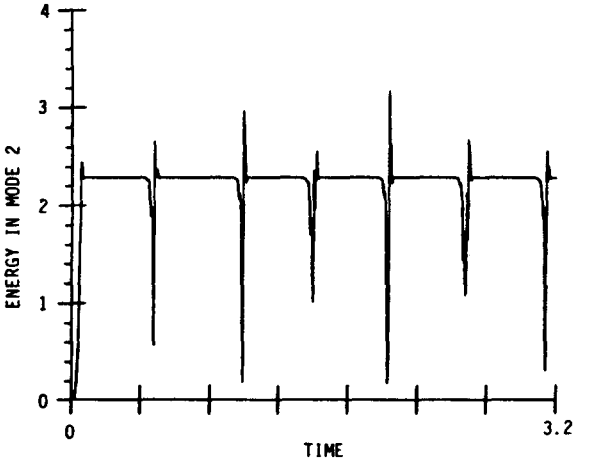

Fig. 3c. The energy in the second mode is nearly constant between the bursts.

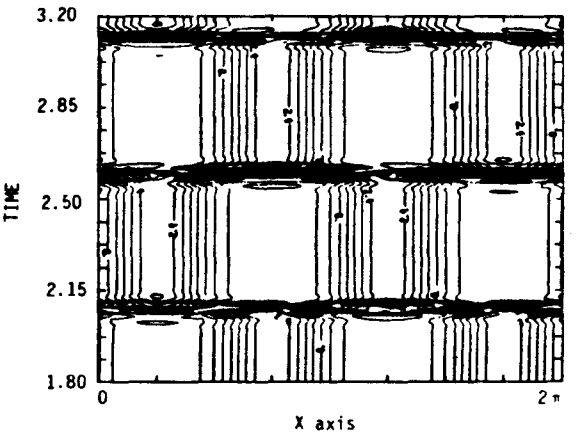

Fig. 3d. The (x, t) contour plot of the solution shows a phase shift at the bursts similar to the one in fig. 2c.

When we lowered the precision of the numerical integrations below 10^{-6} per unit time-step, the homoclinic loop disappeared and the solution locked into the pseudoattracting bimodal fixed point. The precision threshold was below the 10^{-6} energy level necessary to trigger the energy feedback into the odd modes. Pushing precision to 10^{-10} in the fig. 3 calculation ensured that the homoclinic loop was not an artifact. This was the first (among many) examples that alerted us to the extreme sensitivity of the oscillatory solutions to the precision of the numerical method.

A torus also coexists in the range $43 \lesssim \alpha \leq 52$. It starts as T_1 and bifurcates into T_2 at $\alpha \approx 45$. For α slightly larger than 43, the torus is metastable, and the orbit drops onto the homoclinic loop. No direct transition between the bimodal fixed point and a torus has been detected in the neighborhood of $\alpha = 43$. This observation strengthens the homoclinic picture.

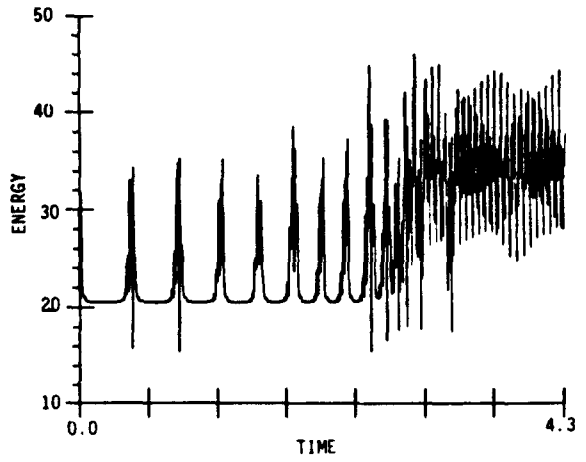

Fig. 4a. The $\alpha = 46$ solution at first bursts with a decreasing frequency and then locks into the T_2 torus.

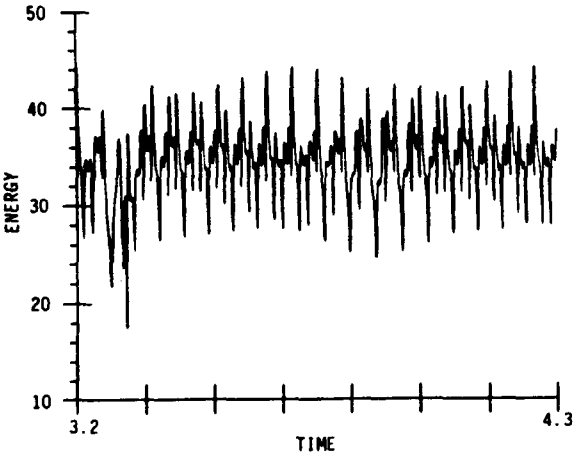

Fig. 4b. Expanded plot of the energy in the solution in fig. 4a.

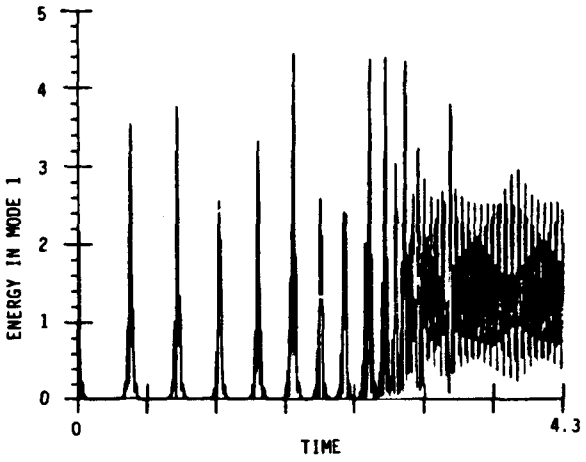

Fig. 4c. The two underlying periods can be seen in the energy of the first mode ($\alpha = 46$).

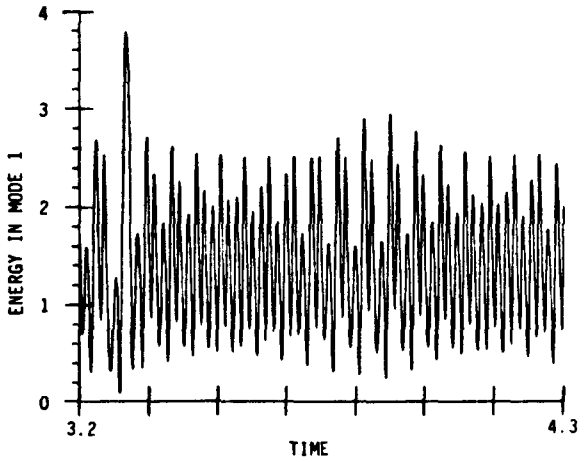

Fig. 4d. Expanded plot of the energy in the first mode in fig. 4c.

In fig. 4 ($\alpha = 46$, $\tilde{L} = 3.40$, $u_0(x) = \cos x + \cos 2x + \cos 3x + \cos 4x$), we show the interplay between the perturbed homoclinic orbit and the attracting torus T_2. The dynamics first take place on a perturbed homoclinic orbit, with less and less time spent in the neighborhood of the hyperbolic point

$$\tilde{u}(x) = 2.15\cos 2x + 0.6\cos 4x + \cdots .$$

At $t \approx 2.8$, the dynamics lock onto a torus T_2. Fig. 4b shows a blowup of the energy evolution for $3.2 \le t \le 4.3$, with the two basic periods $\tau_1 \approx 0.047$ and $\tau_2 \approx 0.58$. The energy in mode 1 (fig. 4c) is even more striking; after bursting more and more frequently away from the 10^{-6} level, it locks into a beating wave with the two basic freqencies τ_1 and τ_2. This can be seen in the plot of the solution in fig. 4d for $t \in [3.2, 4.3]$.

The dynamics on T_2 quickly become more complex with increasing α. An involved quasi-periodic motion occurs as early as $\alpha \approx 47$. However, at $\alpha = 52$ the solution suddenly locks into a traveling

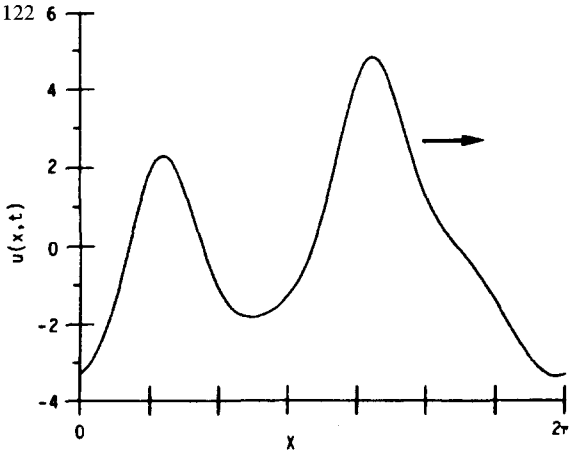

Fig. 5a. Profile of the $\alpha = 52$ traveling wave solution.

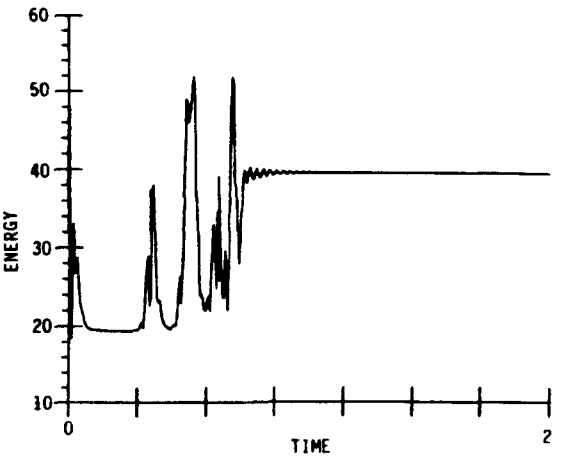

Fig. 5b. The energy in the solution locks into the constant traveling wave value.

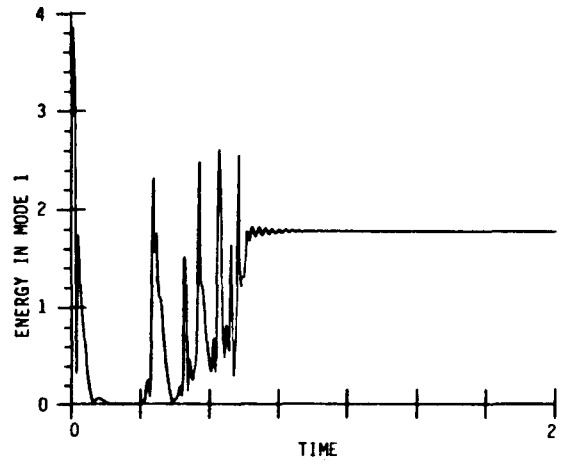

Fig. 5c. Energy in the first mode of the solution ($\alpha = 52$).

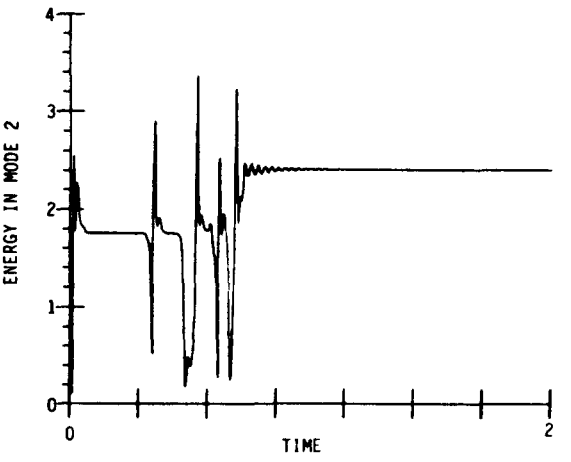

Fig. 5d. Energy in the second mode of the solution ($\alpha = 52$).

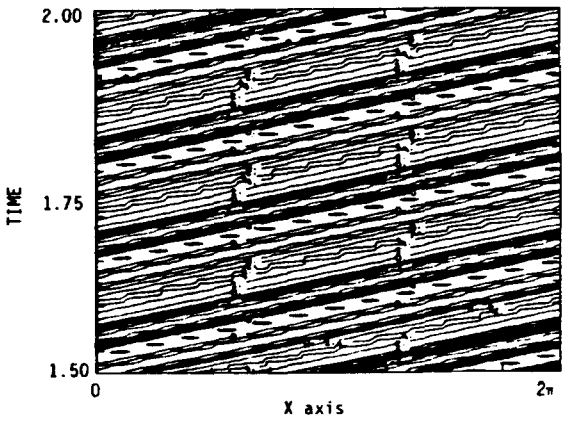

Fig. 5e. The contour plot of the traveling wave solution shows some waves, indicating that it may be only an approximate traveling wave.

wave train. That is, a well-defined wave with a characteristic structure with two humps (fig. 5a) travels at constant speed on the spatial torus $x \in [0, 2\pi]$. Fig. 5 elucidates this structure for $\alpha = 52$, ($\tilde{L} = 3.60$), $u_0(x) = 3\cos x + 3\cos 3x + 0.3\cos 6x$; in an attempt to excite the trimodal fixed point the initial value

$$\tilde{u}(x) = 3\cos 3x + 0.33\cos 6x + \cdots$$

was chosen. This function is a stable fixed point when $\alpha = 50$.

Surprisingly, the transient dynamics first lock onto the previous perturbed homoclinic orbit associated with the bimodal hyperbolic fixed point for $t \in [0, 0.7]$ before locking into the traveling wave train at $t \approx 0.9$ (fig. 5b). Fig. 5c of the energy in the first mode confirms this. It exhibits the characteristic bursts away from the zero level before jumping to a steady level of 1.8. The dynamics of the energy in the even modes, such as mode 2 in fig. 5d, are the mirror image of the odd mode behavior. After a sequence of plateaus at the 1.8 level, energy in the second mode jumps at the steady level of 2.4.

The contour levels of the solution in fig. 5e exhibit the typical wave-train pattern with a period approximately 0.14. The energy is present in all modes in the traveling wave train, which excludes any relation with the bimodal or trimodal fixed points. In fact, by analyzing the solution's behavior for α between 46 and 52, we suspect that the traveling wave train is a special invariant manifold on the torus T_2.

The traveling wave train undergoes a Hopf bifurcation at $\alpha = 53$, $\tilde{L} = 3.64$, and quickly evolves into complicated quasi-periodic motion. A similar two-humped wave train (somewhat steeper) has been observed for $92 \leq \alpha \leq 98$. In the interval $52 \leq \alpha < 54$, initial conditions with the first six cosine and sine modes excited to a level of $\mathcal{O}(1)$ were imposed; the solution displayed persistent near-chaotic behavior without settling into any of the above attractors. We are investigating these cases to determine if the T_2 torus breaks up or if there is a transverse perturbed homoclinic orbit.

We finally present an example of chaos at the onset of the fourth chaotic window $\alpha \geq 117.3$, ($\tilde{L} \geq 5.415$). In fig. 6, we took $\alpha = 117.50$, ($\tilde{L} = 5.42$), and the initial condition $u_0(x) = \sin x + \cos x + \sin 2x + \cos 2x$. The chaotic motions do not reveal any structure until after $t = 1.42$, when we noticed two intermittencies in the chaotic behavior (fig. 6a).

Close inspection of the energy in modes 1 (fig. 6b), 2 (fig. 6c), and 3 (fig. 6d) shows that they drop to a highly oscillatory pattern about a low level;

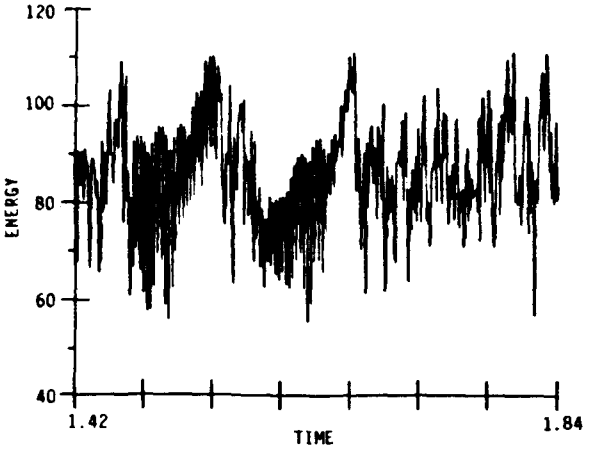

Fig. 6a. The energy in the $\alpha = 117.5$ window is chaotic with intermittent excursions.

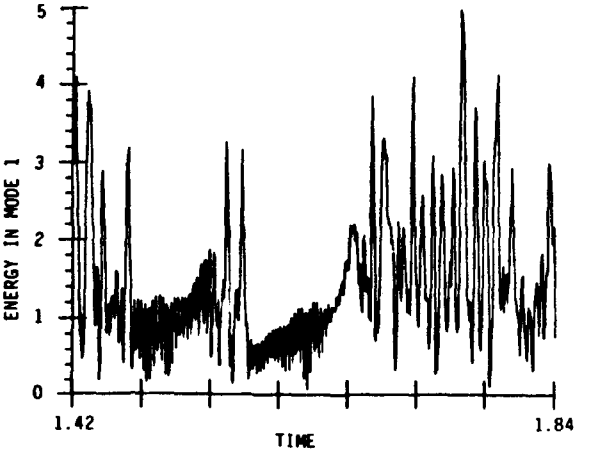

Fig. 6b. The energy in the first mode is small near the fixed point.

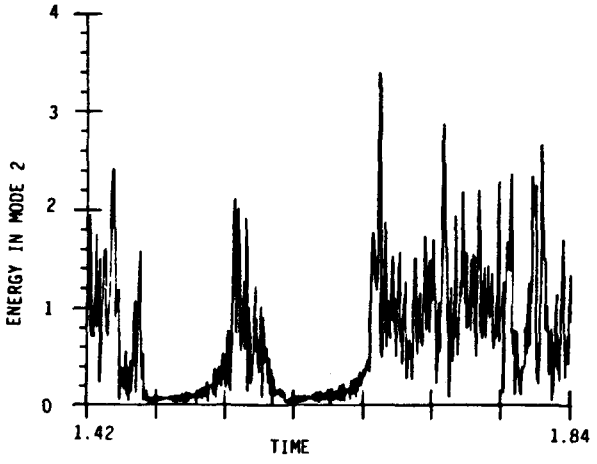

Fig. 6c. Energy in the second mode ($\alpha = 117.5$).

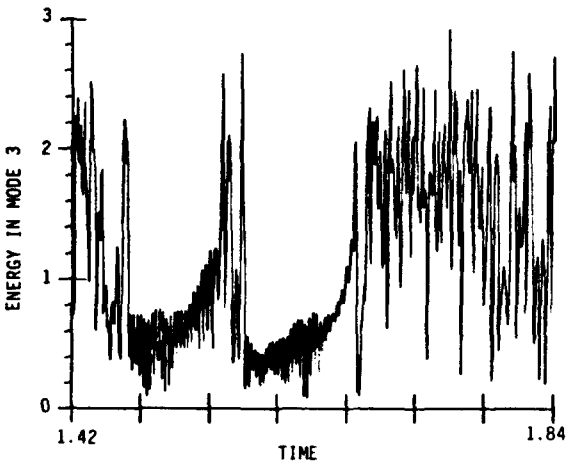

Fig. 6d. Energy in the third mode ($\alpha = 117.5$).

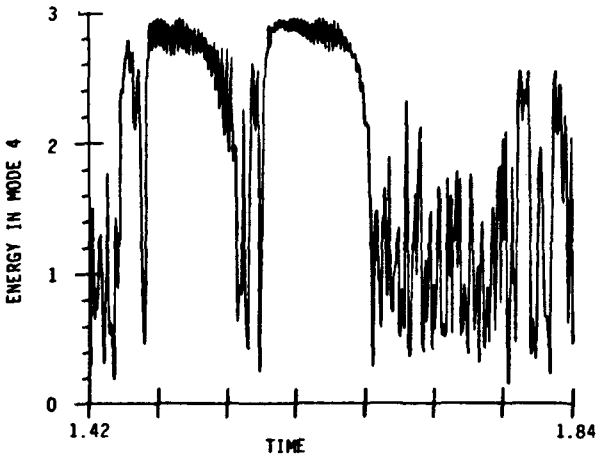

Fig. 6e. The energy in the fourth mode oscillates about the quadrimodal fixed point for $1.5 \le t \le 1.65$.

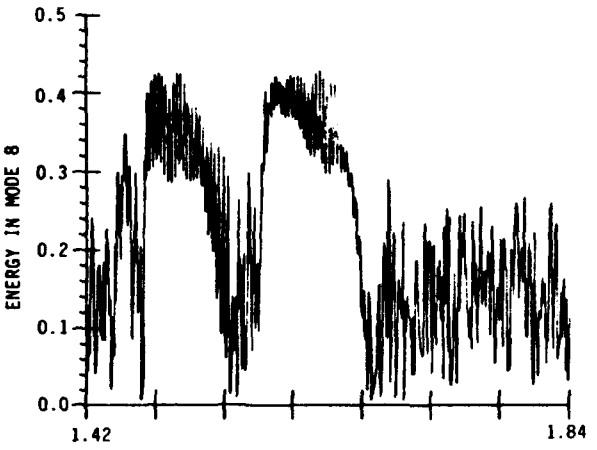

Fig. 6f. The energy in the eighth mode oscillates about the quadrimodal fixed point for $1.5 \le t \le 1.65$.

the same is true for modes 5, 6, and 7. The energy in modes 4 (fig. 6e) and 8 (fig. 6f) jumps to much higher levels during the intermittent bursts. In fact, the orbit seems to be suddenly attracted to the point $\tilde{u}(x) = 3\cos 4x + 0.4\cos 8x + \cdots$, oscillates rapidly in its neighborhood, and suddenly escapes from it. Not unexpectedly, $\tilde{u}(x)$ is the quadrimodal fixed point that became hyperbolic at $\alpha = 117.3$.

Integrating the equations far beyond what is presented here shows that these intermittencies (protracted oscillations in a small neighborhood of the hyperbolic point) do not occur with any periodicity: in fact, they are somewhat sparse and random. We suspect the underlying structure to be a transverse homoclinic orbit. As expected, when we lowered the precision of this calculation to below 10^{-6}, the solution converged to the fixed point and did not escape. We conjecture that this extreme sensitivity to the numerical precision is the reason our results differ from those of Manneville [15].

To complete the homoclinic skeleton, we have observed a metastable torus T_1, for $\alpha = 117.50$

$(u_0(x) = \cos x + \cos 2x + \cos 3x)$, that destabilizes into a similar chaotic motion.

5. Conclusions

The K–S equations bridge the gap between infinite-dimensional behavior of PDEs and the finite-dimensional behavior in dynamical systems of ODEs. The solutions to the K–S equation reveal a complex interplay of simple spatial patterns and low fractal dimensional chaos. Cellular solutions where the jth mode dominates,

$$\tilde{u}_j(x) = a_{1_j} \cos jx + \varepsilon a_{2_j} \cos 2jx + \varepsilon^2 a_{3_j} \cos 3jx + \cdots,$$

affect the chaotic behavior by forming the basis for homoclinic solution orbits. These orbits are imbedded in a maze of invariant tori.

The extreme sensitivity of the simulations to the numerical precision requires error tolerances of less than 10^{-6} and reflects the very small basin of attraction for some of these solution manifolds.

Our current theoretical and numerical work is centered around tracking transverse perturbed homoclinic orbits and broken low-dimensional tori. The theoretical understanding of the bifurcation structure of these inertial manifolds is offering new challenges and revealing an extremely rich structure.

Acknowledgments

Our unravelling of the dynamics of the K–S equation has benefited greatly from discussions with C. Foias, U. Frisch, P. Holmes, N. Koppell, J. Marsden, B. Scheurer, R. Temam and S. Zaleski. This work was supported by the U.S. Department of Energy under contract W-7405-ENG-36 and the Office of Scientific Computing.

References

[1] M.T. Aimar, "Etude numérique d'une équation dévolution non linéaire dérivant l'instabilité thermodiffusive d'un front de flamme," Thèse 3 ème cycle Université de Provence (1982). See also M.T. Aimar and P. Penel, "Quelques Apects Numériques Nouveaux Pour le Modèle de Front de Flamme," Colloque National d'Analyse Numerique, Guidel, France (1983).

[2] A.J. Babchin, A.L. Frenkel, B.G. Levich and G.I. Sivashinsky, "Nonlinear Saturation of Rayleigh–Taylor Instability in Thin Films," Phys. Fluids 26 (1983) 3159–3161.

[3] D.J. Benney, "Long Waves in Liquid Film," J. Math and Phys. 45 (1966) 150–155.

[4] P. Constantin, C. Foias, and R. Temam, "Attractors Representing Turbulent Flows," to appear in Memoirs of the A.M.S. (1985).

[5] C. Foias, G.R. Sell and K. Temam, "Inertial Manifolds for Dissipative Partial Differential Equations," Proc. Acad. Sc. Paris, to appear (1985).

[6] C. Foias, B. Nicolaenko, G.R. Sell and R. Temam, "Inertial Manifolds for the Kuramoto – Sivashinsky Equations," Proc. Acad. Sc. Paris, to appear (1985).

[7] U. Frisch, Z.S. She and O. Thual, "The Kuramoto–Sivashinsky Equations: A Case Study in Elastic Turbulence," Proc. Conf. on Turbulence, Nice (1984), to appear in Springer Verlag Lecture Notes in Physics (1985).

[8] J. Guckenheimer and P. Holmes, Nonlinear Oscillations, Dynamical Systems, and Bifurcation of Vector Fields (Springer, Berlin, 1984).

[9] J.M. Hyman, "Numerical Methods for Nonlinear Differential Equations," in: Nonlinear Problems: Present and Future, A.R. Bishop, D.K. Campbell and B. Nicolaenko, eds. North-Holland, Amsterdam, (1982) pp. 91–107.

[10] J.M. Hyman, "The Method of Lines Solution to Partial Differential Equations," Courant Institute of Mathematical Sciences, Vol. C003007-139 (October 1976).

[11] Y. Kuramoto and T. Tsuzuki, "On the Formation of Dissipative Structures in Reaction–Diffusion Systems," Prog. Theor. Phys. 54 (1975) 687–699.

[12] Y. Kuramoto and T. Tsuzuki, "Persistent Propagation of Concentration Waves in Dissipative Media Far From Thermal Equilibrium," Prog. Theor. Phys. 55 (1976) 356–369.

[13] Y. Kuramoto, "Diffusion-induced Chaos in Reactions Systems," Suppl. Prog. Theor. Phys. 64 (1978) 346–367.

[14] S.P. Lin, "Finite Amplitude Side-Band Stability of a Viscous Fluid," J. Fluid Mech. 63 (1974) 417–429.

[15] P. Manneville, "Lyapunov Exponents for the Kuramoto–Sivashinsky Equations," Proc. Conf. on Turbulence, Nice 1984, to appear in Springer Verlag Lecture Notes in Physics (1985).

[16] D.M. Michelson and G. I. Sivashinsky, "Nonlinear Analysis of Hydrodynamic Instability in Laminar Flames II. Numerical Experiments," Acta Astronautica 4 (1977) 1207–1221.

[17] B. Nicolaenko, B. Scheurer and R. Temam, "Quelques proprietes des attracteurs pour l'équation de Kuramoto–Sivashinsky," C. R. Acad. Sc. Paris 298 (1984) 23–25.

[18] B. Nicolaenko, B. Scheurer and R. Temam, "Attractors for the Kuramoto–Sivashinsky Equations," Physica 16D (1985) 155–183.

[19] B. Nicolaenko, B. Scheurer and R. Temam, "Strange attractors for a Class on Nonlinear Evolution Partial Differential Equations," in preparation.

[20] B. Nicolaenko, B. Scheurer and R. Temam, "Attractors for the Kuramoto–Sivashinsky Equations," AMS-SIAM Lectures in Applied Mathematics 23, to appear (1985).

[21] A. Pumir, "Structures Localisées et Turbulence," Thèse 3 ème cycle, Paris (1982).

[22] A. Pumir, P. Manneville and Y. Pomeau, "On Solitary Waves Running Down an Inclined Plane," J. Fluid Mech. 135 (1983) 27–50.

[23] Y. Pomeau, A. Pumir and P. Pelce, "Intrinsic Stochasticity with Many Degrees of Freedom," preprint C.E.A. S.P.T., Saclay, France (1984).

[24] D. Ruelle, "Characteristic Exponents for a Viscous Fluid Subjected to Time Dependent Forces," Comm. Math. Phys. 92 (1984) 285–300.

[25] G. Sivashinsky, "Nonlinear Analysis of Hydrodynamic Instability in Laminar Flames, Part I. Derivation of basic equations," Acta Astronautica 4 (1977) 1177–1206.

[26] G. Sivashinsky, "On Flame Propagation Under Conditions of Stoichiometry," SIAM J. Appl. Math. 39 (1980) 67–82.

[27] G.I. Sivashinsky and D.M. Michelson, "On Irregular Wavy Flow of a Liquid Down a Vertical Plane," Prog. Theor. Phys. 63 (1980) 2112–2114.